ELSEVIER

www.elsevier.nl/locate/jelechem

Journal of Electroanalytical Chemistry 480 (2000) 133–149

Journal of Electroanalytical Chemistry

A complete numerical simulation of the techniques of alternating current linear sweep and cyclic voltammetry: analysis of a reversible process by conventional and fast Fourier transform methods

D.J. Gavaghan [a,b,c,*], A.M. Bond [c]

[a] *Oxford University Computing Laboratory, Wolfson Building, Parks Road, Oxford OX1 3QD, UK*
[b] *Nuffield Department of Anaesthetics, University of Oxford, Radcliffe Infirmary, Oxford OX2 ONE, UK*
[c] *Department of Chemistry, Monash University, Clayton, Vic. 3168, Australia*

Received 16 August 1999; received in revised form 22 November 1999; accepted 23 November 1999

Abstract

We describe the method of achieving the first completely general simulation of ac linear sweep and cyclic voltammetry making use of the fully implicit Richtmyer modification (FIRM) method. The simulation technique is applied to a reversible process under conditions where a sinusoidal waveform of any amplitude is superimposed onto the dc potential which is swept at a finite scan rate. Results, where possible, are compared with the existing theory derived at constant dc potential to confirm the fidelity of the simulation. In particular, we demonstrate excellent agreement with the results of Engblom et al. [J. Electroanal. Chem. xxx (1999) xxx] for large amplitude ac voltammetry described in the companion paper immediately preceding this article. The use of conventional and Fourier transform methods of data analysis are compared to highlight the advantages of the use of the fast Fourier transform algorithm in ac voltammetry.

Keywords: Numerical simulation; Ac voltammetry; Cyclic voltammetry

1. Introduction

Linear sweep and cyclic voltammetry, in their direct current (dc) modes, represent the most commonly employed techniques for elucidating mechanisms of electrode processes at macrodisc electrodes [1]. In the linear sweep form, the potential is swept over the range of interest at a known scan rate and the current is measured as a function of applied potential (time). In the cyclic form of the technique, the potential direction of the scan is switched at a pre-determined value and the potential is scanned back to the initial (or some other) value. Thus, a triangular dc voltage, E_{dc}, is employed in cyclic voltammetry. The dependence of the voltammetric response on scan rate, v, and other variables such as the switching potential provides a means of probing the kinetics of an electrochemical process (homogeneous and heterogeneous steps), and frequently for the calculation of the thermodynamics of the reaction (reversible potential and equilibrium constants). Numerous methods are available to simulate dc voltammograms and commercial solution packages are now available for the task [2,3].

In principle, a far more powerful approach to studying mechanisms of electrode processes is to use alternating current (ac) versions of dc linear sweep or cyclic voltammetry [1,4–6]. In these techniques, an alternating potential (E_{ac} or ΔE) of known angular frequency (ω) is superimposed onto the waveform used in the dc techniques, and the ac response is then measured as a function of dc potential and angular frequency to extract the kinetics and thermodynamics. Consequently, a great deal of information additional to that available in dc voltammetry can be obtained.

The advantages of ac linear sweep and ac cyclic voltammetry over their dc counterparts have been summarised by Bard and Faulkner [1]. However, unfortu-

* Corresponding author. Fax: +61-3-99054597.
E-mail address: gavaghan@comlab.ox.ac.uk (D.J. Gavaghan)

0022-0728/00/$ - see front matter
PII: S0022-0728(99)00476-3

nately, theoretical solutions to the ac techniques are very limited compared to the dc case [1,4–6]. Furthermore, where solutions are available, suppositions commonly have been invoked which require that the dc and ac time scales are resolvable, and that the amplitude of the applied alternating potential is very small so that the theoretical solution may be linearised. Effectively, the first requirement means that dE_{dc}/dt ($=v$, the dc sweep rate) $\ll dE_{ac}/dt$ ($=\omega\Delta E$, the product of the amplitude, ΔE, and angular frequency, ω of the ac signal) or at $t \gg 0$, $\omega \gg vnF/RT$, in order that the dc potential can be assumed to be constant for the duration of the superimposition of the ac signal. The perceived need to linearise the problem means that usable values of ΔE have usually been restricted to the mV region in most theoretical studies [7].

This second requirement of small amplitudes has been elegantly overcome by the recent analytical work of Engblom et al. [8], described in the companion paper immediately preceding this article, which we became aware of whilst preparing this manuscript. The mutually complementary nature of our researches prompted our request to the Editor that these articles be published consecutively.

However, the first problem of requiring resolvable time domains remains, and in order to have access to an ac voltammetric solution of equal validity to that presently available with dc techniques, a complete numerical simulation of the ac and dc components of the experiment clearly is required. Until recently, computing power to address a simulation of this kind was not readily available. Thus, computing limitations severely restricted the scope of initial simulations in ac voltammetry made over 20 years ago [9]. However, advances in efficiencies that can be achieved with simulation of the relevant partial differential equations coupled with the speed of computers now present in most laboratories should mean that the complete simulation of ac techniques should be tractable without the need to invoke any approximations related either to values of ΔE or overlapping time domains.

On the basis of the advantage of greater access to computation power, we have decided to reconsider the mathematical modelling of ac voltammetry to ascertain advantages that may accrue from having a solution as general as that routinely available in dc techniques. Of course, the greater speed of computers also implies that far more sophisticated data treatments based on fast Fourier transform (FFT) analysis in the frequency domain are also now available, so that the full power of data analysis strategies not applicable to the time domain also can be conveniently employed.

In the present paper, we therefore provide a method which can achieve the first completely general numerical simulation of ac voltammetry. The technique in the present instance is applied to a reversible process, and results, where possible, are compared with analytical theory derived with (Refs. [8,9]), and without (Ref. [10]), the constant dc potential approximation to confirm the fidelity of the simulation. Finally, the use of conventional and Fourier-transform methods of data analysis are compared to highlight the advantages of the use of the FFT algorithm [1,11]. Other workers have used the FFT form of analysis in impedance spectroscopy (see Refs. [12,13], for example), again employed at constant dc potential, whilst recent studies related to ac voltammetry highlight the relative simplicity of the use of the FFT method of data analysis in modern forms of instrumentation [14,15].

At the end of the paper we compare the results of our numerical simulations for large amplitude ac voltammetry to the analytic results given by Engblom et al. [8] in the companion paper.

2. Methods

Throughout this paper we will consider the case of a macro-electrode so that we can assume that diffusion is a one-dimensional process and, therefore we can compare our numerical results to previously described analytical solutions [7,8,10,16–19]. We therefore consider that semi-infinite mass transport occurs to a planar electrode and that the electrochemical oxidation reaction

$$\mathrm{A} = \mathrm{B} + n\mathrm{e}^- \tag{1}$$

takes place at the electrode surface. Mass transport to the electrode is then modelled by the linear diffusion equation for each species s

$$\frac{\partial c_s}{\partial t} = D_s \frac{\partial^2 c_s}{\partial x^2} \tag{2}$$

where x is the distance from the electrode surface, t is time, and $c_s(x,t)$ is the concentration, and D_s the corresponding diffusion coefficient of each of the species $s = \mathrm{A}$, B. Note, however, that the simulation method need not be restricted to planar diffusion and could readily be extended to the case of radial diffusion at a microdisc electrode.

2.1. Boundary conditions

Assuming semi-infinite linear diffusion conditions hold, the following boundary and initial conditions result

$$\begin{array}{lll} x = 0 & D_\mathrm{A}\dfrac{\partial c_\mathrm{A}}{\partial x} = -D_\mathrm{B}\dfrac{\partial c_\mathrm{B}}{\partial x}, & D_\mathrm{A}\dfrac{\partial c_\mathrm{A}}{\partial x} = k_\mathrm{f}c_\mathrm{A} - k_\mathrm{b}c_\mathrm{B} \\ x \to \infty & c_\mathrm{A} = c_\mathrm{A}^* & c_\mathrm{B} = 0 \end{array} \tag{3}$$

Here, k_f and k_b are the potential dependent rate constants for the forward and backward reactions and are given by

$$k_f = k_0 \exp\left(-\frac{\alpha nF}{RT}[E(t) - E^\circ]\right) = k_0 e^{-\alpha\tau}$$

$$k_b = k_0 \exp\left((1-\alpha)\frac{nF}{RT}[E(t) - E^\circ]\right) = k_0 e^{(1-\alpha)\tau} \quad (4)$$

where $E(t)$ is the applied potential, k_0 is the heterogeneous charge transfer rate constant at standard potential E° and α is the charge transfer coefficient. τ is defined below in Eq. (5). c_A^* is the bulk concentration of species A.

Since, in this paper, the primary goals are to demonstrate the general applicability and accuracy of our methods in comparison to previous approximate analytic theory, we will assume equal diffusion coefficients and fully reversible charge transfer in all simulations, but it is of course obvious that cases involving unequal diffusion coefficients and slow electron transfer are equally tractable. In this special case ($D_A = D_B = D$ with c_B initially absent), it is straightforward to show that $c_B = c_A^* - c_A$, and we need only solve for species A, with the corresponding simplification of the boundary conditions. We will also use a value of k_0 in Eq. (4) which is sufficiently high to ensure that reversible conditions apply, as detailed below. The computer codes are currently written to allow slow electron transfer and non-zero concentrations of c_B, but not unequal diffusion coefficients.

2.2. Non-dimensional variables

We first introduce the following non-dimensional variables related to distance (X), time (τ), and concentration (u_A),

$$X = x/l \qquad \tau = \theta(E_i + vt - E^\circ)$$

$$u_A = c_A/c_A^* \quad (5)$$

where l is some natural length scale, specified below, E_i is the initial potential, and $\theta = nF/RT$.

Substitution of each of these variables into Eq. (2) gives

$$\frac{\partial u_A}{\partial \tau} = \left(\frac{D}{\theta v l^2}\right)\frac{\partial^2 u_A}{\partial X^2} \quad (6)$$

We then choose the length scale l to be

$$l = \sqrt{\left(\frac{D}{\theta v}\right)}. \quad (7)$$

and Eq. (6) simplifies to become

$$\frac{\partial u_A}{\partial \tau} = \frac{\partial^2 u_A}{\partial X^2}, \quad (8)$$

subject to boundary conditions

$$\begin{aligned} &\text{at } X = 0 \quad \frac{\partial u_A}{\partial X} = \Lambda'[u_A e^{-\alpha\tau} - (1-u_A)e^{(1-\alpha)\tau}] \\ &\text{as } X \to \infty \quad u_A = 1 \end{aligned} \quad (9)$$

where $\Lambda' = k_0 l/D$ is a dimensionless rate constant [20], which we take to be equal to 10^6 throughout this paper to ensure fully reversible conditions.

2.3. Calculation of the current

The current, $I(t)$, at the electrode surface is given by

$$I(t) = nFAD\left(\frac{\partial c_A}{\partial x}\right)_{x=0} \quad (10)$$

In non-dimensional variables this becomes

$$I(\tau) = nFAdc_A^* l^{-1/2}\left(\frac{\partial u_A}{\partial X}\right)_{X=0}. \quad (11)$$

A non-dimensional current is therefore given by

$$I^*(\tau) = \left(\frac{\partial u_A}{\partial X}\right)_{X=0} = I(\tau)/[nFac_A^*(\theta v D)^{1/2}], \quad (12)$$

and it is this quantity that we will refer to as the simulated current throughout this paper. For linear sweep voltammetry in non-dimensional variables this definition gives a peak current of 0.4463 at a τ value of 1.109 (see Bard and Faulkner [1] p. 218). The current for an ac signal is non-dimensionalised in identical fashion.

2.4. Applied potential for ac voltammetry

The non-dimensional time τ was defined above to be $\tau = \theta(E_i + vt - E^\circ)$, where E_i is the initial potential. τ can also be thought of as a non-dimensional potential (since it is a function of the product of time t and sweep rate v). A particularly attractive representation for simulation of ac voltammetry arises by imposing the applied potential using the function

$$E(\tau) = \tau + \Delta\tau \sin(\Omega\tau) \quad (13)$$

where Ω is the non-dimensional angular frequency, and $\Delta\tau$ is the amplitude of the oscillation. This allows us to define the rate of oscillation in the ac component in terms of the total number of oscillations, N, say, in a complete dc sweep. The duality in the interpretation of τ as either non-dimensional time or non-dimensional potential creates a slight problem in interpretation of results from non-dimensional variables in terms of dimensional variables. Below we therefore give what we believe is the simplest method of translating from non-dimensional to dimensional variables and vice versa, making use of the fact that N must be the same in each case.

2.5. Relationship between non-dimensional and dimensional variables

Throughout this paper we will simulate for values of τ from -10 to 10, which corresponds to sweeping from -0.2569 to $0.2569/n$ V relative to $E°$ in dimensional variables at 25°C. If we define these non-dimensional and dimensional potential ranges as τ_r and E_r, respectively, then we wish to ensure that we have the same number of oscillations, N, over each of the two ranges. Since the range of the potential is not affected by the standard or initial potentials, τ_r and E_r are related by

$$E_r = \frac{1}{\theta}\tau_r. \tag{14}$$

In non-dimensional variables, the period of each oscillation is $\mathscr{T} = \tau_r/N$, and the angular frequency $\Omega = 2\pi/\mathscr{T}$. In dimensional variables, we must take into account the sweep rate v: the total time of the experiment is E_r/v (in s), and so the period $T = E_r/(vN)$, and the dimensional angular frequency $\omega = 2\pi/T$. Since the number of oscillations over the complete dc sweep in both dimensional and non-dimensional variables is the same we obtain the relationship between the two periods as:

$$\frac{\tau_r}{\mathscr{T}} = N = \frac{E_r}{vT} \tag{15}$$

Re-arranging and substituting for E_r from Eq. (14) gives

$$T = \frac{\mathscr{T}}{\theta v}, \text{ for the period, and}$$

$$\omega = \theta v \Omega \text{ for the angular frequency.} \tag{16}$$

The amplitude of the ac component must also be in the same ratio to the range of the potential in both dimensional and non-dimensional variables. That is,

$$\frac{\Delta\tau}{\tau_r} = \frac{\Delta E}{E_r} \tag{17}$$

Again substituting for E_r from Eq. (14) gives

$$\Delta E = \frac{\Delta\tau}{\theta}. \tag{18}$$

A concrete example might make this clearer. Assuming values of $n = 1$ and a temperature of 25°C (so $\theta = nF/RT = 38.92\ \mathrm{V}^{-1}$), the range of τ values we will use, -10 to 10 (so $\tau_r = 20$), corresponds to sweeping from -0.2569 V ($= -10/38.92\ \mathrm{V}^{-1}$) to 0.2569 V relative to $E°$. If $N = 40$ i.e. we have 40 complete oscillations, then the period $\mathscr{T} = \tau_r/N = 20/40 = 1/2$, and angular frequency $\Omega = 4\pi$. Assuming a sweep rate of 0.1 V s^{-1}, in dimensional variables this gives a dimensional period of $T = \mathscr{T}/\theta v = 0.128$ s, corresponding to an angular frequency, ω, of about 50 rad s^{-1}. If the amplitude of the non-dimensional applied signal is $\Delta\tau = 0.3$, this corresponds to a dimensional value of $\Delta E = 0.3/38.92\ \mathrm{V}^{-1} = 7.7$ mV.

2.6. Numerical methods

The one-dimensional linear diffusion equation and associated boundary conditions given above are solved numerically using a 6-level FIRM algorithm as described by Feldberg and Rudolph and co-authors [21–24] and the reader is referred to these papers for fuller details. This simulation is used in conjunction with a simple exponentially expanding mesh. The simulated current is calculated from the concentration values using a three-point, second-order finite difference approximation (see for example [25]).

2.7. Comparison with analytical results

Previous analytical results have suggested that provided the dc potential is held constant, at say E_{dc}, during the time that the ac signal is applied, then the system should have [7] the following properties:

- The peak of the ac wave at a particular angular frequency ω (which we will denote by I_p), should be linear, within experimental error [7], in ΔE for amplitudes $\leq 8/n$ mV (assuming $n = 1$ this is equivalent to $\Delta\tau < 0.3$ in our non-dimensional variables).
- I_p should be linear in $\omega^{1/2}$ (in the region in which it is linear, within experimental error [7], in ΔE).
- The phase shift between the applied potential and the fundamental harmonic ac wave should be 45°.
- If we consider the ac wave in terms of its harmonics, then the currents associated with the first (or fundamental) and second harmonics at small amplitudes [6,7] and other approximations referred to above, are given, in dimensional variables, by:

$$I(\omega) = \frac{n^2F^2Ac_A^*(\omega D)^{1/2}\Delta E}{4RT\cosh^2(j/2)}\sin\left(\omega t + \frac{\pi}{4}\right) \tag{19}$$

$$I(2\omega) = \frac{2^{1/2}n^3F^3Ac_A^*(\omega D)^{1/2}(\Delta E)^2\sinh(j/2)}{16R^2T^2\cosh^3(j/2)}\sin\left(2\omega t - \frac{\pi}{4}\right) \tag{20}$$

where $j = (nF/RT)(E_i - E°)$. The above expressions can all be non-dimensionalised as described earlier to give

$$I(\Omega) = \frac{\Delta\tau\sqrt{\Omega}}{4\cosh^2(\tau/2)}\sin\left(\Omega\tau + \frac{\pi}{4}\right) \tag{21}$$

$$I(2\Omega) = \frac{\Delta\tau^2\sqrt{2\Omega}\,\sinh(\tau/2)}{16\cosh^3(\tau/2)}\sin\left(2\Omega\tau - \frac{\pi}{4}\right) \tag{22}$$

and we will compare our numerical results to these non-dimensional equivalents.

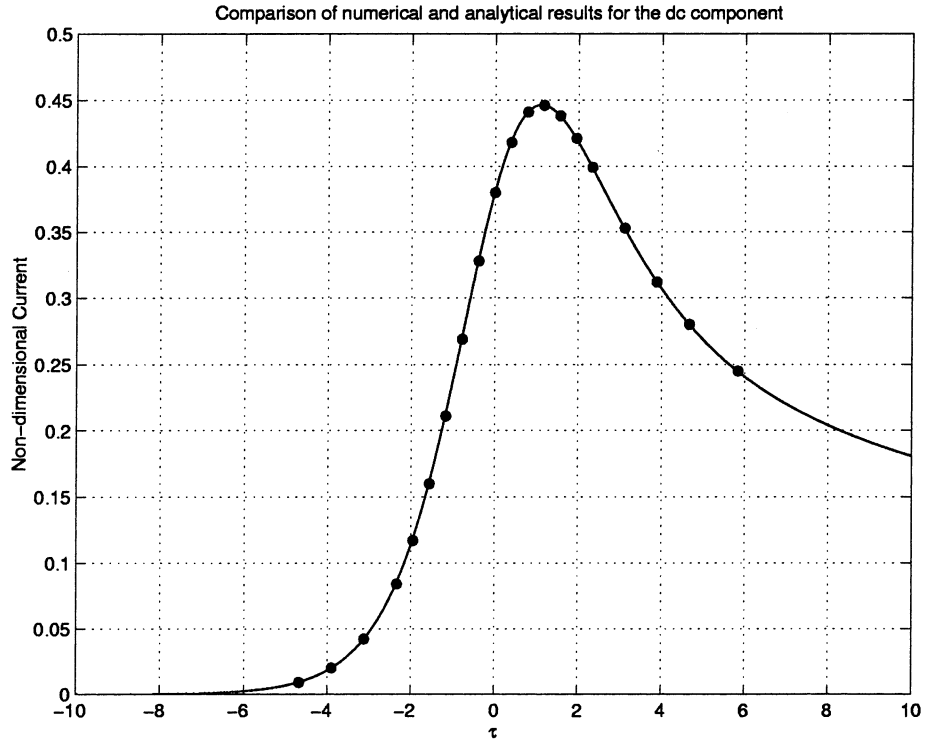

Fig. 1. The full line gives the simulated current calculated using the FIRM method, and the points are taken from table 6.2.1 of Ref. [1] for fully reversible charge transfer.

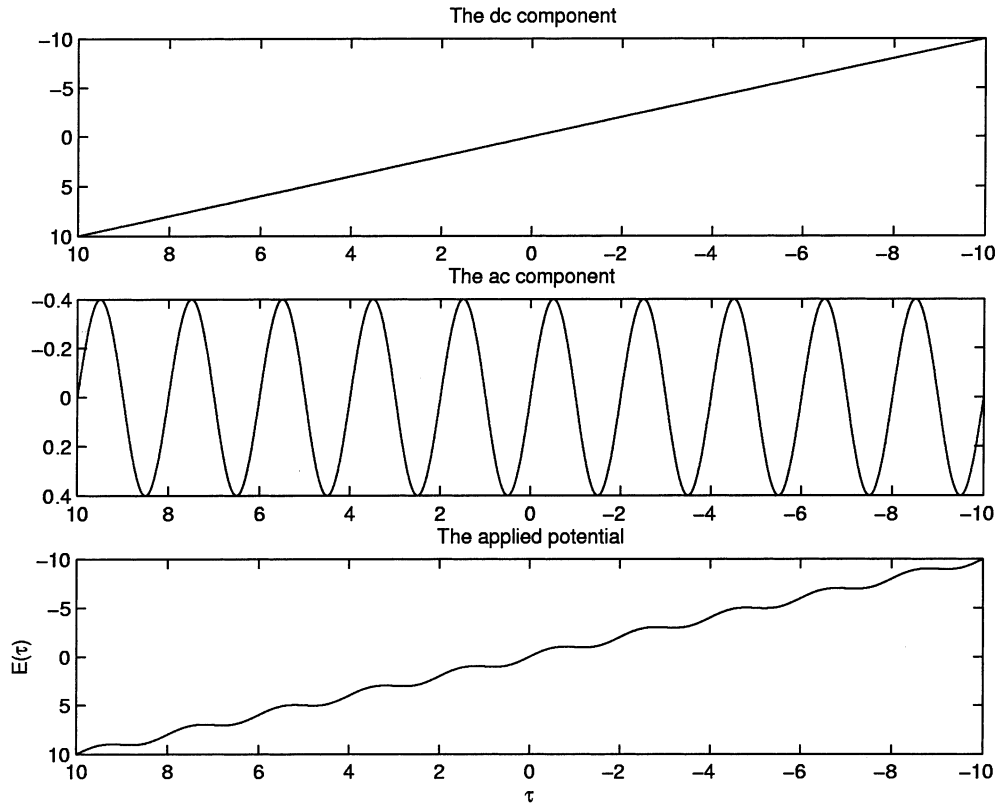

Fig. 2. The upper graph shows the dc component of the applied potential, the central graph the ac component with $\Omega = \pi$ and $\Delta\tau = 0.4$ as defined in Eq. (13), and the lower graph the combined applied potential.

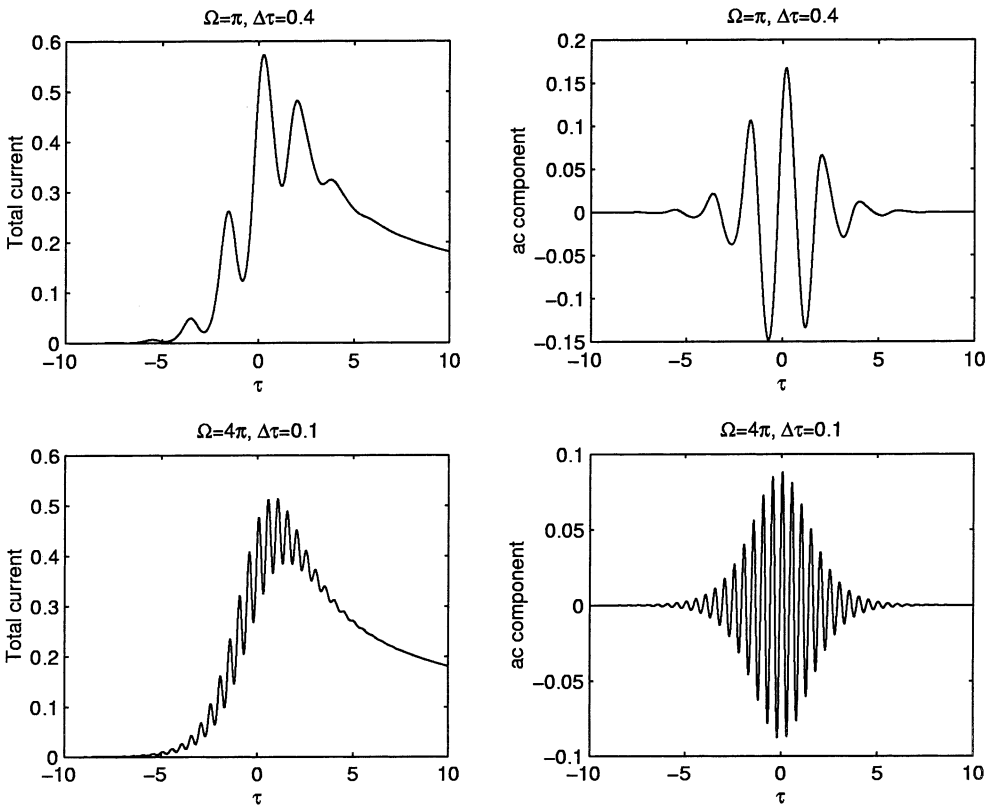

Fig. 3. Illustrative results of the numerical simulations for a very slow oscillation (upper panels), and a more rapid oscillation (lower panels). We also use a larger amplitude of $\Delta\tau = 0.4$ in the upper panels, and 0.1 in the lower panels.

Table 1
Correspondence between the non-dimensional angular frequency Ω and its dimensional equivalent ω (in rad s^{-1}) assuming a sweep rate of 0.1 V s^{-1}

Ω	0.25π	0.5π	π	2π	4π	8π	16π	32π	64π
ω/rad s^{-1}	3.06	6.11	12.23	24.45	48.91	97.82	195.6	391.3	782.5

In Section 3 we will use the following methods, each equivalent to a previously used experimental approach, to determine whether or not our simulation techniques also give the above properties:

1. (a) Subtracting the dc component from the combined signal to obtain the ac wave.
   (b) Using a dc-filter to obtain the ac wave.
2. Using the fast Fourier transform (FFT) algorithm.

3. Results

3.1. Testing the 1-D code

We use a simple expanding mesh designed to give extremely good accuracy for the dc component, which we compare to the analytic values given in table 6.2.1 of Bard and Faulkner [1]. In order to obtain a numerical solution, the semi-infinite region $[0, \infty)$ is replaced by the finite region $[0, X_{max}]$, and we follow Britz [26] in choosing X_{max} to be $\max(1.0, 6\sqrt{D\tau})$ (since beyond this distance all concentration values will effectively equal the bulk concentration). This solution region is then discretised by choosing a minimum mesh spacing, say δX_0, and an expansion factor $r \geq 1$, and our 1-D mesh has nodes at the points

$$X_i = r^i \delta X_0, \quad \text{for } i = 1, \ldots, M. \tag{23}$$

r and δX_0 are chosen to give the desired level of accuracy, and M is chosen to ensure that the total coverage of the mesh is greater than X_{max}. Numerical experimentation revealed that values of $\delta X_0 = 0.025$ and $r = 1.01$ gives a peak current of 0.44630 at $\tau = 1.11$ using a timestep of $\delta\tau = 0.01$ or 2000 timesteps. The

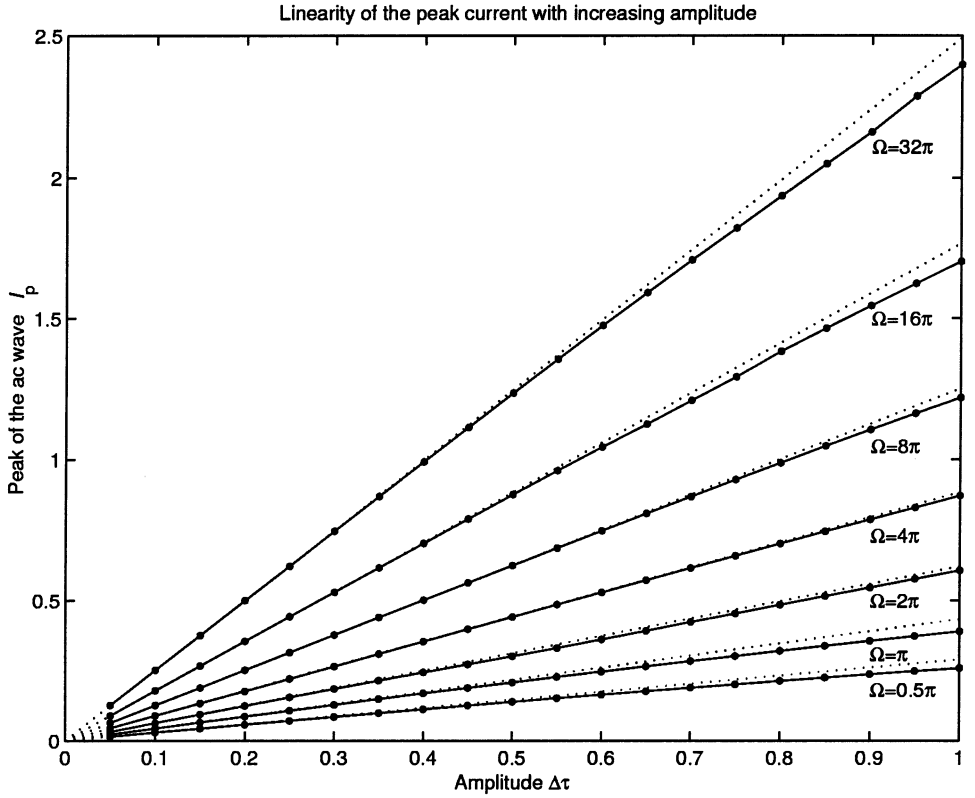

Fig. 4. Dependence of the peak current of the ac wave with increasing amplitude, $\Delta\tau$, for values of the angular frequency, Ω from 0.5π up to 32π. True linearity is given by the dashed line, whilst the points joined by a full line show the simulated values of the peak ac component.

results are compared to the analytical results in Fig. 1. For the simulations of ac voltammetry, we need to use slightly finer meshes and smaller timesteps. We have found that ensuring that there are at least 100 timesteps in each complete oscillation of the ac component ensures time accuracy. The finest spatial mesh that we use has $\delta X_0 = 0.003125$ and $r = 1.01$ gives a maximum value of $M = 419$.

3.2. Incorporating the ac component

The applied potential, τ, for the linear sweep, the ac component, and the combined signal for ac voltammetry are shown in Fig. 2. For clarity, we have shown a fairly slow, large-amplitude oscillation with ten complete cycles over the range of τ values of -10 to 10, which corresponds to a value of $\Omega = \pi$ in Eq. (13) above, and an amplitude $\Delta\tau = 0.4$. This actually represents an example where conditions required for published analytic solutions to be valid would not be met, except for the solution given in Ref. [16]. Assuming a sweep rate of 0.1 V s^{-1}, this would correspond to an angular frequency of about 12 rad s^{-1}, and an amplitude of about 12 mV. The results of the numerical simulation using this particular parameter set is shown in the upper left panel of Fig. 3, which shows the combined dc + ac signal. At this low angular frequency, the distortion to the ac component is large. This is emphasised in the upper right panel of Fig. 3, where we have subtracted the dc signal (shown in Fig. 1) to give the ac signal. In the lower panels of Fig. 3 we show the results of using an angular frequency $\Omega = 4\pi$, and an amplitude $\Delta\tau = 0.1$ (about 50 rad s^{-1}, and 2.5 mV assuming a sweep rate of 0.1 V s^{-1}), and here we see that we are moving towards a symmetric ac wave of the kind predicted under conditions where the analytic solutions are valid [6,7,18][1].

In the following sections of this paper, we will consider values of Ω ranging from 0.25π up to 64π. For reference purposes, we therefore give in Table 1 the corresponding frequencies in rad s^{-1} assuming a sweep rate of 0.1 V s^{-1}.

3.3. Subtracting the dc component from the signal to obtain the ac wave

All of the results in this subsection are obtained by subtracting the numerically simulated dc component

[1] Previous analytical work on ac voltammetry has termed the envelope containing the positive part of the ac component the ac wave.

from the numerically simulated combined signal to obtain the ac wave. This then allows us to analyse the ac component in isolation and obtain very accurate results for comparison with analytical results derived by earlier workers.

3.3.1. Linearity with amplitude

The dependence of the peak current, I_p, with increasing amplitude $\Delta\tau$ is considered in Fig. 4, for values of Ω ranging from 0.5π to 32π (i.e. from 5 to 320 full oscillations over the range of τ). As can be seen, at all values of Ω shown, very good linearity is obtained in the range $0 \leq \Delta\tau \leq 0.4$ (corresponding to amplitudes between 0 and 10 mV) as predicted from the analytical theory. Importantly, this linearity is maintained at very low frequencies such as $\Omega = 0.5\pi$ ($\omega \sim 6$ rad s^{-1}), where the approximation ($v \ll \Delta\tau\Omega$ and $\omega \gg vnF/RT$) suggested to be a requirement for the approximate analytical theory to hold, is not met. However, this result is in agreement with extended theory that accommodates consideration of the overlapping time domains [9,16]. In contrast, linearity at high amplitude is not maintained (see later).

3.3.2. Dependence of I_p on $\Omega^{1/2}$

The results shown in Fig. 5 illustrate the dependence of the peak current of the ac wave on $\Omega^{1/2}$. It can be seen that except at very low frequencies ($\Omega < 2\pi$), the peak current is both linearly dependent on $\Omega^{1/2}$ and gives excellent agreement with the sum of the first two harmonics of the analytic solution. All simulations presented in Fig. 5 used a value of $\Delta\tau = 0.1$ which is well within the linear range illustrated in Fig. 4.

3.3.3. The phase shift

The phase shift between the applied potential and the resulting ac component is illustrated in Table 2 for increasing values of the angular frequency Ω. For val-

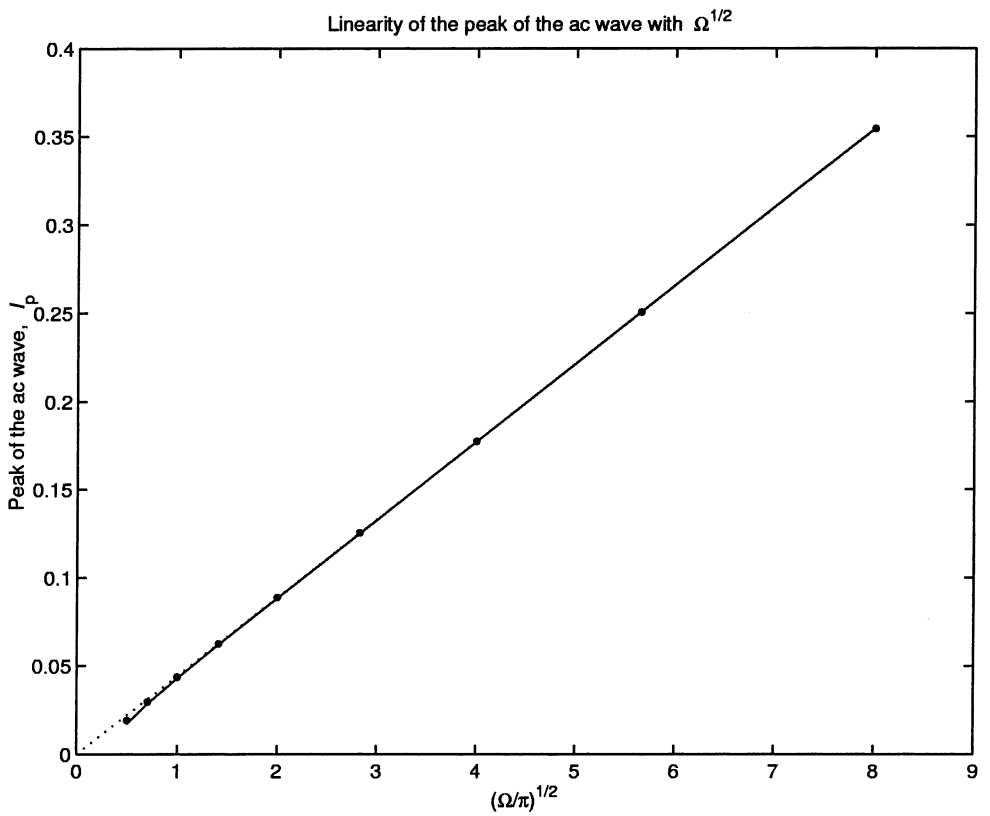

Fig. 5. Dependence of the peak current of the ac wave on the square root of angular frequency, $\Omega^{1/2}$, for values Ω from 0.25π up to 64π. The numerical simulation results are given by the full line and used a value of $\Delta\tau = 0.1$. The points were obtained by taking the maximum of the sum of the first two harmonics of the analytic solution of Eqs. (21) and (22). The dashed line gives true linearity.

Table 2
The phase shift between the applied potential and the resulting ac component for values of Ω between 0.25π and 64π

Angular frequency, Ω	0.25π	0.5π	π	2π	4π	8π	16π	32π	64π
Phase shift	66.3	55.4	48.8	46.2	45.4	44.9	45.0	45.0	45.0

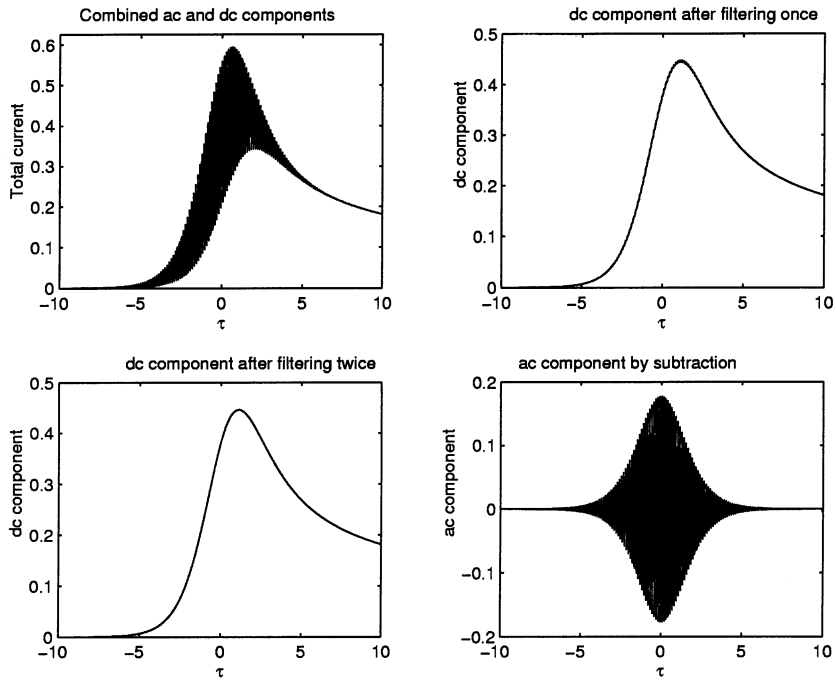

Fig. 6. The results of dc filtering for angular frequency $\Omega = 16\pi$: the upper left panel shows the combined signal; the upper right panel shows the results of filtering the signal once using a moving average; the lower left shows the results of applying the same filter again — also shown in this graph is the original background signal, and it is clear that on this scale the filtered signal and the true dc component are indistinguishable; and the lower right panel shows the ac wave obtained by taking the difference between the upper left and lower left graphs.

ues of $\Omega > 4\pi$ the numerical simulation gives excellent agreement with the analytical value of 45° (valid when the dc and ac time domains do not overlap). For values of $\Omega \leq 4\pi$ the phase shift increases: further consideration of the upper panels of Fig. 3 suggest that this is due to the increasing distortion (due to the non-linearities in the background signal) of the ac component at lower frequencies. In a later section we will show that this is also manifested in an overlap in the frequency spectra of the dc and ac components at low frequencies.

3.4. Using a filter to remove the dc component to obtain the ac wave

All of the results described in the previous section were obtained by subtracting the simulated dc signal from the combined dc plus ac signal. However in practice, conventional forms of ac instrumentation would record only the combined signal which could then be filtered to obtain the dc and ac components. We show below that at the higher frequencies ($\Omega > 4\pi$) where the period of the ac component is much less than the width of the dc wave, a simple moving average filter[2] can be used to recover the dc component of the signal, which can then in turn be subtracted from the combined signal to give the ac component. This is illustrated in Fig. 6 which shows this process for $\Omega = 16\pi$.

In Table 3 we show the phase angles and peaks obtained from the filtered ac signals (after filtering once and twice), together with the values calculated in the previous section by subtracting the exact background signal (see Table 2 and Fig. 5). Throughout we have again used a value of $\Delta\tau = 0.1$ which is well within the linear range. It is clear that the values of the phase and peak current recovered after filtering the combined signal twice are very accurate.

3.5. Fourier analysis

In principle, separation of dc and ac components of the signal could be undertaken instrumentally via use of a lock-in amplifier [27]. However, the alternative technique that we will consider for analysing the combined signal is Fourier analysis where we will use the fast Fourier transform or FFT to transform from the time domain into the frequency domain [28]. In all of the following results the MATLAB [29] mathematical software package will be used to perform the FFT analyses. This technique is illustrated in Fig. 7, where we show the power spectra of both the background signal, and the combined dc plus ac signal for the case $\Omega = 4\pi$.

[2] Since we know both the angular frequency of the ac component and the sampling rate we can choose to take an average over exactly half a period to either side of interest, so that we get excellent results from filtering just twice.

Table 3
The phase angles and peak currents obtained from the filtered ac signals (after filtering once and twice), together with the values calculated in Section 3.3 by subtracting the exact background signal (and given in Fig. 5 and Table 2)

Angular frequency, Ω	π	2π	4π	8π	16π	32π	64π
Phase shift (from Table 2)	48.8	46.2	45.4	44.9	45.0	45.0	45.0
Phase shift (signal filtered once)	77.5	46.1	45.4	45.1	45.1	45.0	45.0
Phase shift (signal filtered twice)	66.7	45.3	45.4	45.1	45.1	45.0	45.0
Peak current (from Fig. 5)	0.0431	0.0610	0.0882	0.1250	0.1773	0.2508	0.3545
Peak current (signal filtered once)	0.0670	0.0665	0.0901	0.1266	0.1789	0.2530	0.3578
Peak current (signal filtered twice)	0.0891	0.0693	0.0901	0.1256	0.1772	0.2505	0.3546

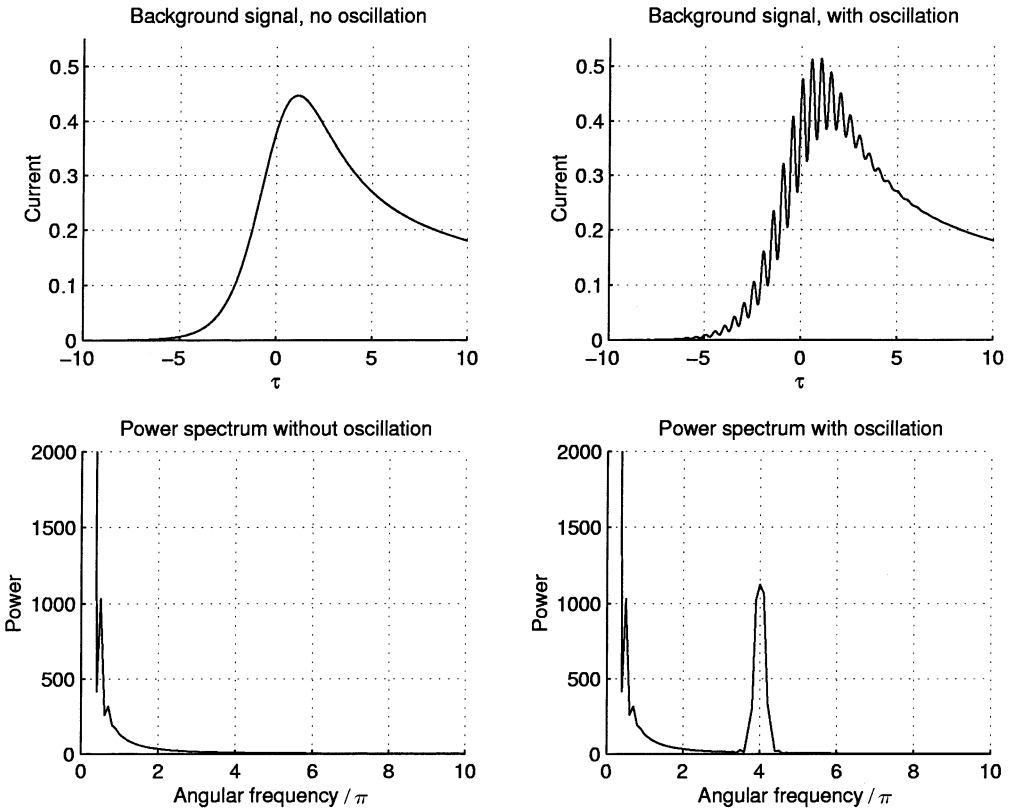

Fig. 7. Illustrative results of Fourier analysis of the dc (left panels), and combined dc plus ac for $\Omega = 4\pi$ (right panels).

It is apparent that there is a small level of overlap between the power spectra of the dc and ac signals for $\Omega = 4\pi$ and $\Delta\tau = 0.1$. This overlap is illustrated more clearly in the upper left panel of Fig. 8 which shows the power spectrum of the combined signal with $\Omega = 2\pi$, $\Delta\tau = 0.1$. In the upper right panel of Fig. 8, we show the same spectrum greatly magnified and in the angular frequency range 3π–5π, to illustrate the presence of the second harmonic. For this very low angular frequency there is a large overlap between the dc spectrum and both the first and second harmonics of the ac spectrum, and we might expect very poor resolution if we attempted to recover either harmonic by filtering.

In the lower panels of Fig. 8 we show similar spectra for $\Omega = 8\pi$, $\Delta\tau = 0.1$. Here there is very little overlap, so that the dc spectrum will have little influence on the first harmonic of the ac spectrum, but will still have a significant effect on the second harmonic. At higher frequencies, the dc spectrum has very little effect on either the first or second harmonics of the ac component. At the higher frequencies examined, the third harmonic can also be observed even at this small amplitude, as illustrated for $\Omega = 64\pi$, $\Delta\tau = 0.1$ in Fig. 9. It is therefore clear that at higher frequencies, we can straightforwardly filter out the dc signal to obtain the ac component, and we can also use filtering to obtain the individual harmonics of the ac component. However, even for an angular frequency of $\Omega = 64\pi$, the power in the second harmonic is extremely small compared to the first harmonic (four orders of magnitude),

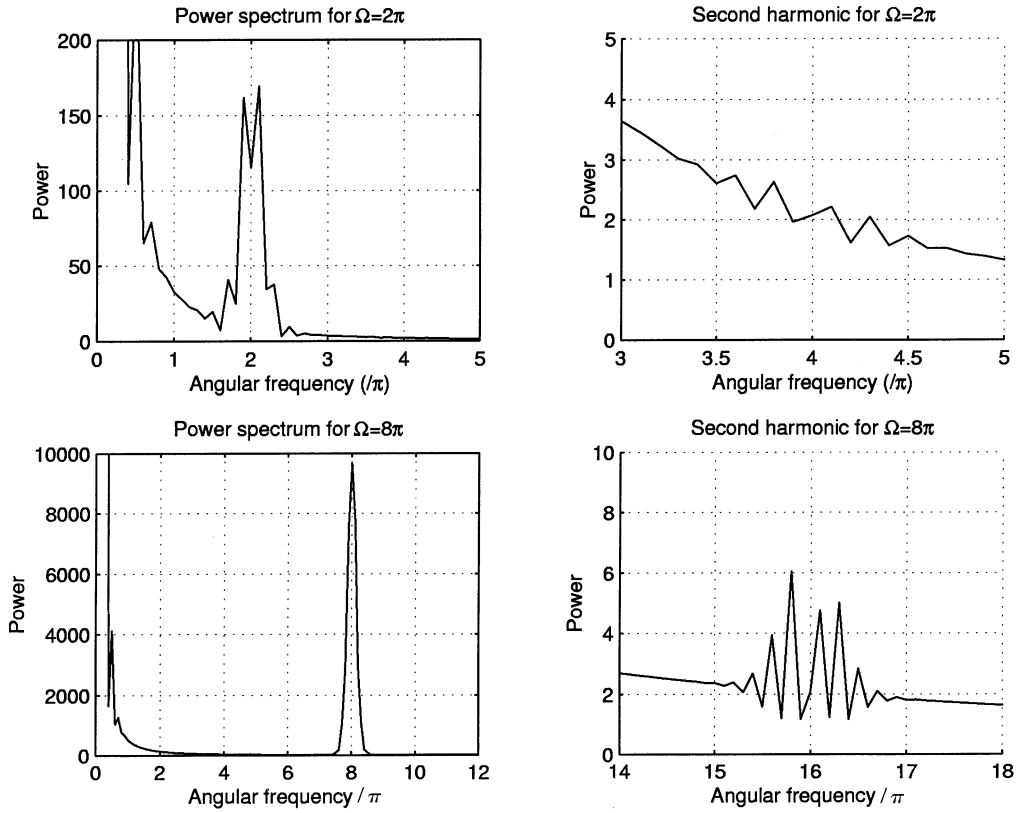

Fig. 8. The power spectra of the first and second harmonics for $\Omega = 2\pi$ (upper panels) and $\Omega = 8\pi$ (lower panels), all with $\Delta\tau = 0.1$.

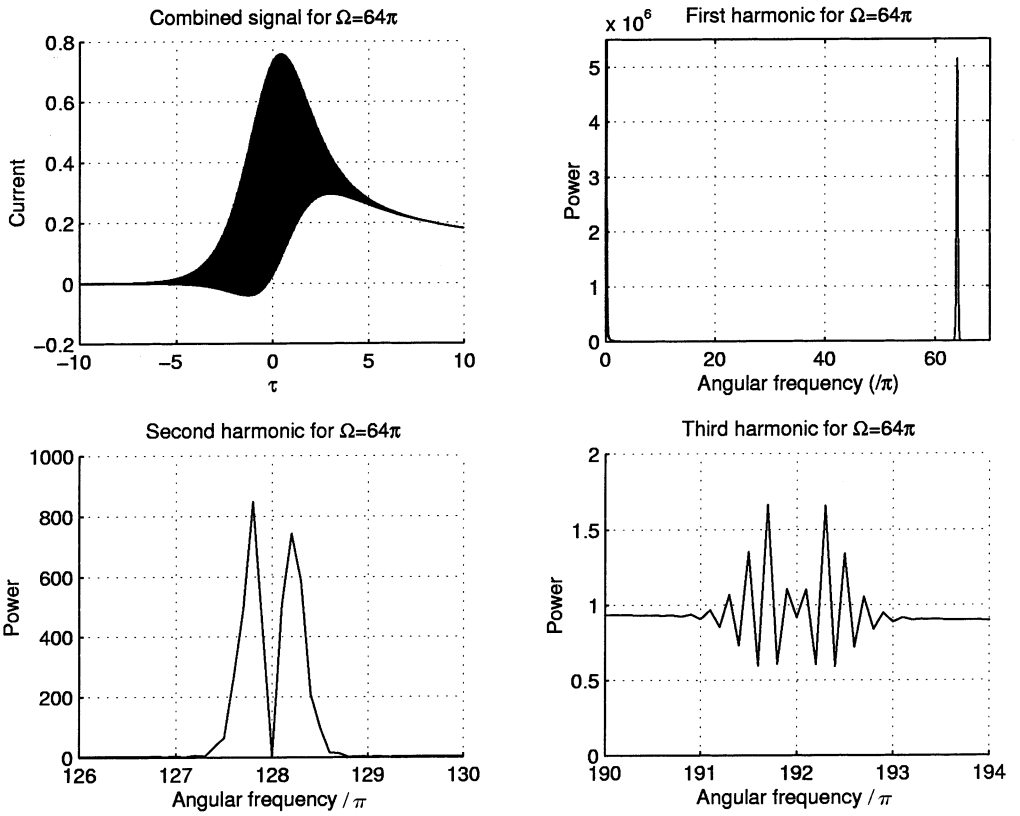

Fig. 9. The combined dc plus ac signal (upper left panel), and its power spectrum at the first, second and third harmonics for $\Omega = 64\pi$ with $\Delta\tau = 0.1$.

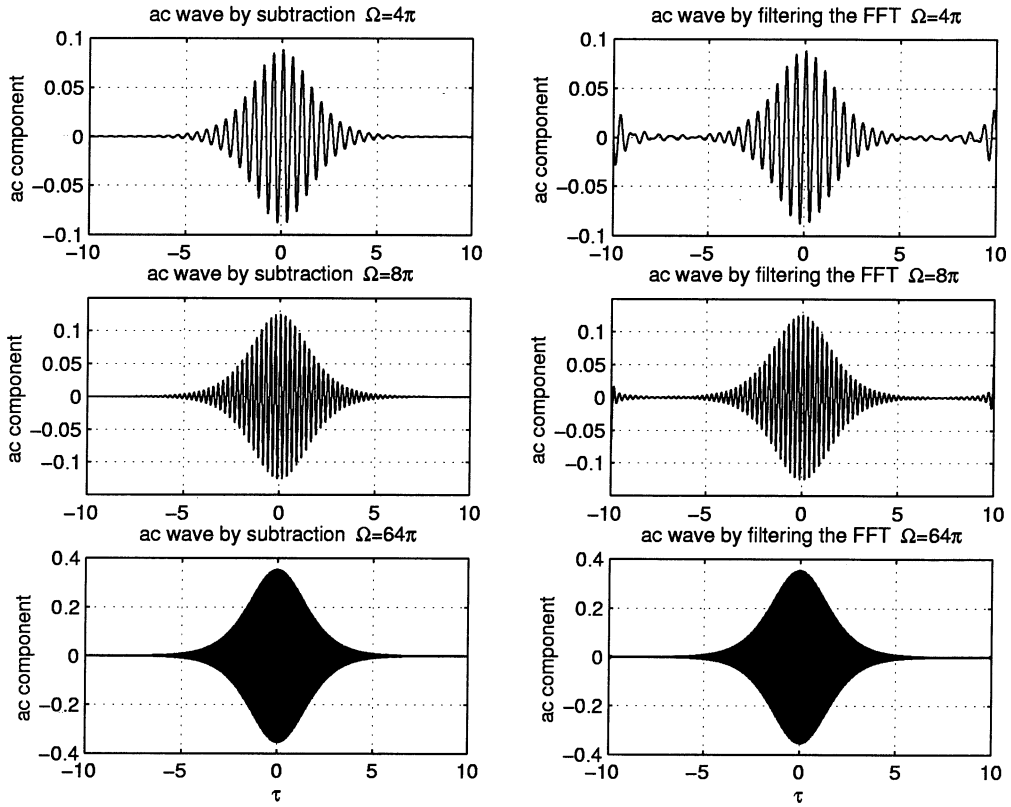

Fig. 10. The left panels show the ac waves obtained by subtracting the simulated dc component from the combined dc plus ac signal, as described in Section 3.3, whilst the right panels show the results of using FFTs to obtain the ac wave as described in the text. In all cases $\Delta\tau = 0.1$.

Table 4
The phase shift and peak current of the ac wave obtained using the subtraction method of Section 3.3 and the FFT method

Angular frequency, Ω	4π	8π	16π	32π	64π
Phase shift (from Table 2)	45.4	44.9	45.0	45.0	45.0
Phase shift from FFT ac wave	45.2	44.9	45.1	45.0	45.0
Peak current (from Fig. 5)	0.0882	0.1250	0.1773	0.2508	0.3545
Peak current from FFT ac wave	0.0879	0.1250	0.1771	0.2505	0.3543

and this is also clear in the lack of symmetry in the lower left panel of Fig. 9. We will show in Figs. 11 and 12 that increasing the amplitude of the applied potential greatly increases the power in the second and third harmonics, allowing them to be recovered accurately by filtering the FFT.

This very efficient filtering procedure is illustrated in Fig. 10 for $\Omega = 4\pi$, 8π, and 64π, again with $\Delta\tau = 0.1$ in all cases. The left panels of Fig. 12 show the ac waves obtained by subtracting the simulated dc component from the combined dc plus ac signal, as described in Section 3.3, whilst the right panels show the results of taking the FFT of the combined signal, setting all components of the FFT up to the first harmonic equal to zero, and then taking the inverse FFT. It is clear that this process has recovered the ac wave very well for all three frequencies, although for $\Omega = 4\pi$, the interaction between the dc and ac term has introduced some errors at the edges of the sampling interval (these errors at the ends of the interval are also present to a lesser extent in recovered waves for $\Omega = 8\pi$ and 64π). The accuracy with which the FFT analysis recovers the ac wave is also reflected in the values of the peak current and phase of the ac waves shown in Table 4. Clearly, provided the frequency is sufficiently high to allow a separation between the spectra of the dc and ac components in the frequency domain, then using the FFT method of analysis we can straightforwardly deconvolute the signal into its ac and dc components in the time domain.

3.5.1. Recovery of higher harmonics using FFTs

We can also recover the higher harmonics by filtering the FFT appropriately before inverting, as illustrated in

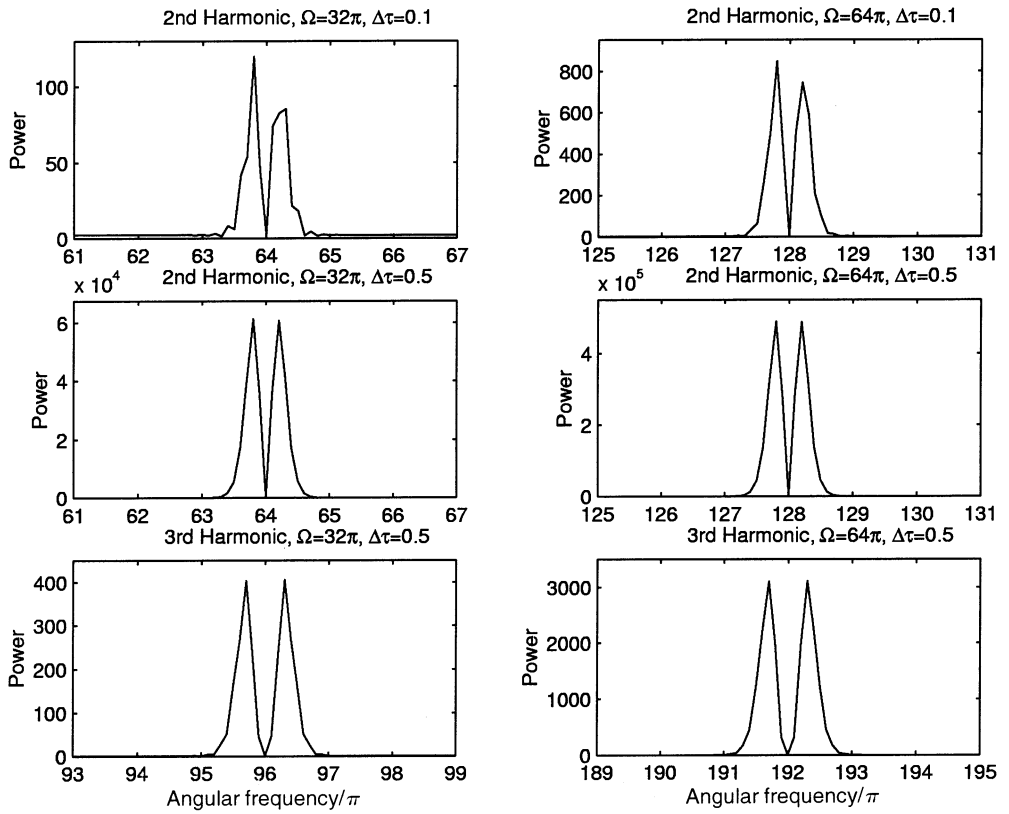

Fig. 11. The power spectra of the second and third harmonics using the FFT method for $\Omega = 32\pi$ and 64π. The upper panels show spectra of the second harmonic for $\Delta\tau = 0.1$. The central panels show the spectra of the second harmonic for $\Delta\tau = 0.5$, whilst the lower show spectra of the third harmonic for $\Delta\tau = 0.5$.

Fig. 12 for $\Omega = 32\pi$ and 64π. Throughout the preceding sections, we have used $\Delta\tau = 0.1$ for the amplitude of the applied potential. This small amplitude gives a very small and poorly defined second harmonic as illustrated in the upper panels of Fig. 11, and this is poorly recovered by the FFT method as shown in the upper panels of Fig. 12. If we increase this amplitude to $\Delta\tau = 0.5$, then we greatly increase the amplitude and definition of both the second and third harmonics, as illustrated in the lower panels of Fig. 11. Under these larger amplitude conditions we obtain much more accurate recovery of both harmonics using the FFT method as illustrated in the central and lower panels of Fig. 12. Thus, for $\Delta\tau = 0.5$, we find the peak and phase lag of the second harmonics to be $I_p = 0.084$ and 45.0° for $\Omega = 32\pi$, and $I_p = 0.119$ and 45.0° for $\Omega = 64\pi$, which agree very closely with the values of $I_p = 0.085$ and $I_p = 0.120$, and a phase lag of 45°, given by the analytic Eq. (22) above.

In contrast, if we repeat the same procedure using the data for $\Delta\tau = 0.1$, we obtain values of $I_p = 0.00176$ from the FFT recovered signal for $\Omega = 32\pi$ which is very inaccurate compared to $I_p = 0.00341$ given by the analytic Eq. (22). For $\Omega = 64\pi$ we still obtain the acceptably accurate value of $I_p = 0.00486$ from the FFT recovered signal, compared to $I_p = 0.00482$ for the analytic value. So, for $\Omega = 64\pi$, we observe the expected 25-fold increase in the FFT recovered I_p values in going from $\Delta\tau = 0.1$ to 0.5.

4. Cyclic ac voltammetry

It is also straightforward to simulate cyclic ac voltammetry in the same manner as for the linear sweep ac technique. We have analysed both the forward and backward sweeps (at all harmonics) for a range of values of Ω and found, as expected, that for a completely reversible reaction the ac waves for the forward and backward sweeps are identical [6] but of opposite signs. In Fig. 13, we show the power spectra of both the forward (full line) and backward (dashed line) sweeps for ac cyclic voltammetry with $\Omega = 16\pi$ and $\Delta\tau = 0.1$. It is clear that the spectra of the ac components are coincident. All of the preceding results for ac linear sweep voltammetry are therefore also valid for ac cyclic voltammetry.

5. Large amplitude ac voltammetry

In the companion paper, Engblom et al. [8] have derived an analytic solution for large-amplitude ac

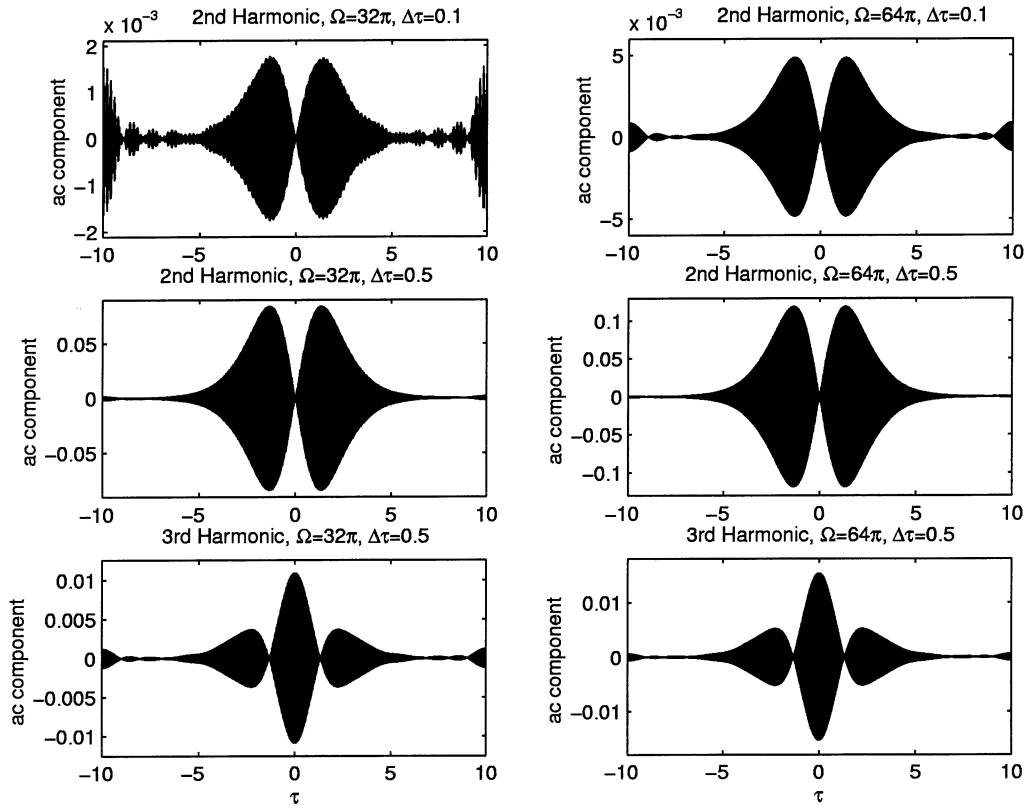

Fig. 12. Recovery of the second and third harmonics using the FFT method. The upper panels show the second harmonic recovered from a signal with $\Delta\tau = 0.1$. The central panels show the second harmonic recovered from a signal with $\Delta\tau = 0.5$, whilst the lower show the third harmonic recovered from a signal with $\Delta\tau = 0.5$.

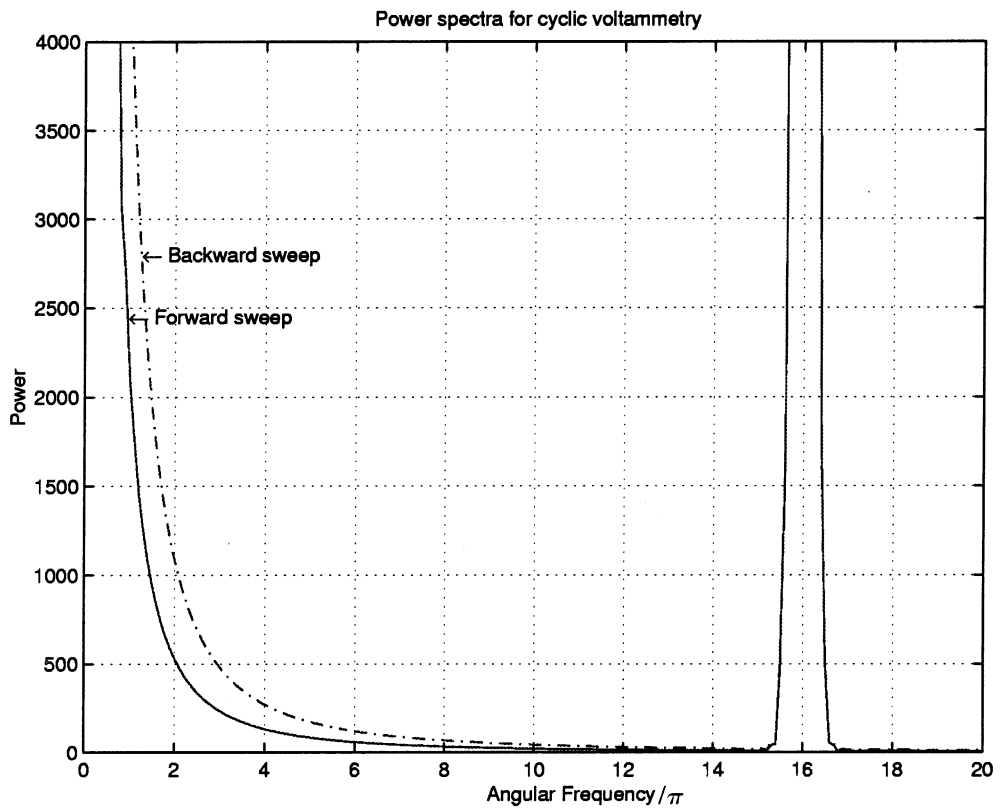

Fig. 13. The power spectra of the forward (full line) and backward (dashed line) sweeps for ac cyclic voltammetry with $\Omega = 16\pi$ and $\Delta\tau = 0.1$.

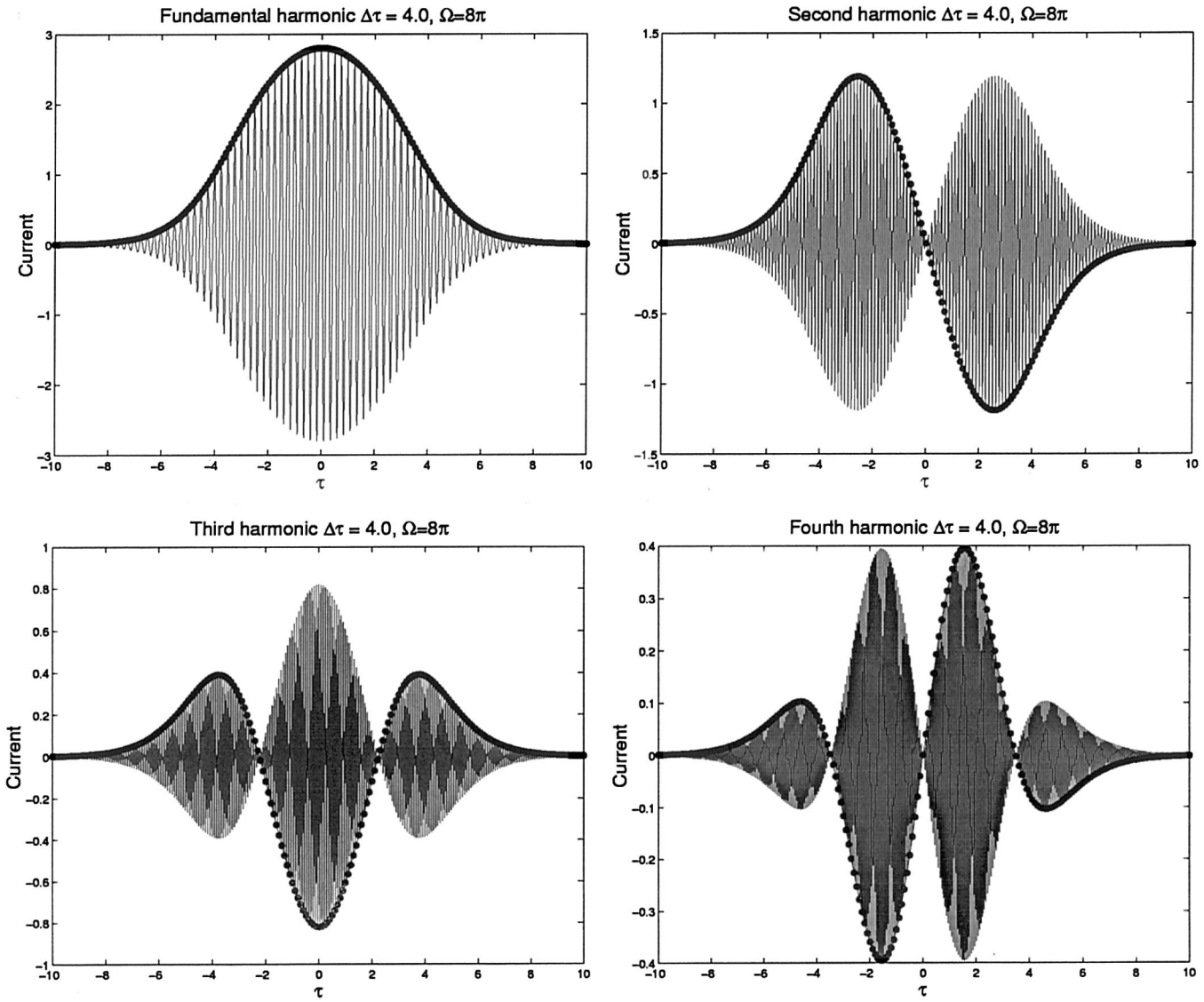

Fig. 14. Comparison of the ac harmonics recovered from the numerical simulation by FFT filtering (oscillating full lines), with the analytic solution for the envelope given in the accompanying paper [8] (dots joined by full line).

voltammetry, assuming a constant dc potential for the duration of the ac signal (see Eq. (16) of that paper). These authors have shown that as the amplitude increases, the ac wave includes significant contributions from the higher harmonics of the fundamental frequency (Ω), and the peak current of the first harmonic of the ac wave is attenuated, and is no longer linear in $\Delta\tau$.

We have compared the results that we have obtained using our simulation method for ac linear sweep voltammetry combined with FFT analysis to recover this first harmonic at values of $\Omega = 8\pi$ and 16π with those given by Engblom et al.'s [8] analysis for values of $\Delta\tau$ from 0.0625 to 16 (corresponding to approximately 1.5 to 400 mV for $n = 1$ at $T = 298$ K), and the results are given in Table 5. It can be seen that, as with the small amplitude oscillations, we obtain excellent agreement with the analytical results.

Engblom et al. [8] have also given analytic results for the envelope containing the fundamental ac harmonic and the higher harmonics at large amplitudes (see sections 4.1, 4.2 and 4.3 and figures 4 and 5 of the companion paper [8]). Since, at large amplitudes, the power in the ac signal for the higher harmonics is much greater, we can also recover these higher harmonics from our simulated data. In Fig. 14, we have done this for the fundamental, second, third and fourth harmonics for the case $\Delta\tau = 4.0$ and $\Omega = 8\pi$. The oscillating full line is calculated using FFT filtering of our simulated current, whilst the points joined by a full line which form the envelope were calculated from Eq. (32) of the companion paper together with the FFT methods de-

Table 5
Comparison of the peak current of the fundamental ac wave obtained by numerical simulation and FFT analysis, with the analytic theory of Oldham given in Eq. (16) of the accompanying paper

$\Delta\tau$	Simulated peak current	Analytic peak current
$\Omega = 8\pi$		
0.0625	0.0783	0.0781
0.125	0.1563	0.1565
0.25	0.3117	0.3120
0.5	0.6164	0.6169
1	1.180	1.181
2	2.033	2.034
4	2.801	2.802
8	3.102	3.136
16	3.170	3.171
$\Omega = 16\pi$		
0.0625	0.1106	0.1105
0.125	0.2211	0.2214
0.25	0.4410	0.4414
0.5	0.8719	0.8727
1	1.669	1.670
2	2.876	2.878
4	3.963	3.964
8	4.387	4.436
16	4.482	4.484

scribed in sections 4.1, 4.2 and 4.3 of that paper [8][3]. Agreement is again excellent in all cases.

6. Computing

All codes are written in Fortran and were run on a Sun Workstation (Spare Ultra 30 with a 300 MHz processor). The computation to calculate the background signal which used parameter values of $\delta X_0 = 0.025$ and $r = 1.01$, giving a maximum value of $M = 248$, and a timestep of $\delta\tau = 0.01$ or 2000 timesteps took less than 1 s of CPU time. The longest computation for $\Omega = 64\pi$, used values of $\delta X_0 = 0.003125$ and $r = 1.01$, giving a maximum value of $M = 449$, and 64000 timesteps (100 per oscillation), and took 25 s of CPU time. The FFTs and graphics were performed using MATLAB [29]. All codes are available from the authors upon request.

[3] Since Engblom et al. [8] have treated the dc component as constant, the natural scaling of the current used in figure 4 of the companion paper is different to the one that we have used. The relationship between the two is

$$I_{\mathrm{EMO}} = \frac{4}{\Delta\tau\sqrt{\Omega}} I_{\mathrm{GB}}$$

where I_{EMO} is the scaled current used in figure 4 of [8], IGB is our simulated current, and $\Delta\tau$ in our notation is equivalent to nFV/RT in the EMO notation.

7. Conclusions

We have introduced a new approach to provide a complete numerical simulation of ac voltammetry which includes provision for a finite scan rate, large amplitudes, and solutions to problems more complicated than the reversible case presented here. For each of the methods of analysis considered with the reversible case we have been able to demonstrate excellent agreement with analytical results derived previously, which assumed a constant dc potential and non-overlapping dc and ac time domains.

It is clear that the most powerful analytical tool is provided by the FFT method of analysis. For this method we have shown that provided that the frequency of the ac component is sufficiently high to allow a separation between the spectra of the dc and ac components in the frequency domain, then the FFT method allows us, straightforwardly, to decompose the signal into its ac and dc components in the time domain. Provided that there is sufficient power in the ac component in the frequency domain (i.e. the ac signal has a sufficiently large amplitude or frequency), then the FFT method also allows us to recover the higher harmonics of the ac signal accurately.

Finally, we have shown that the simulation technique works equally well for linear sweep and ac cyclic voltammetry, covers the large amplitude case for which analytical theory is given in the companion paper [8], and can be used to simulate the response when the dc potential is not constant. Thus, experimental strategies can now be based on knowledge gained from a perfectly general numerical simulation treatment requiring no small amplitude or overlapping time domain approximations. Moreover, it now follows that since dc simulations are available for all electrode geometries and mechanisms, that the same will now be true with respect to ac voltammetry since previous limitations based on inadequate computing power [9] have now vanished.

Acknowledgements

The authors are pleased to acknowledge the financial support of the Australian Research Council for a Special Investigator Award for AMB, and the Medical Research Council of Great Britain for a Career Development Fellowship for DJG, which has allowed them to undertake this research.

References

[1] A.J. Bard, L.R. Faulkner, Electrochemical Methods, Wiley, New York, 1980.

[2] M. Rudolph, D.P. Reddy, S.W. Feldberg, Anal. Chem. 66 (1994) 589A.
[3] D.K. Gosser Jr., Cyclic Voltammetry: Simulation and Analysis of Reaction Mechanisms, VCH, New York, 1993.
[4] P.H. Rieger, Electrochemistry, second ed., Chapman and Hall, New York, 1994, p. 366.
[5] M.A. Brett, A.M.O. Brett, Electrochemistry: Principles, Methods and Applications, Oxford University, Oxford, 1993, pp. 238–241.
[6] A.M. Bond, Modern Polarographic Methods in Analytical Chemistry, Marcel Dekker, New York, 1980, pp. 341–349.
[7] D.E. Smith, in: A.J. Bard (Ed.), Electroanalytical Chemistry, Marcel Dekker, New York, 1966, pp. 1–149.
[8] S.O. Engblom, J.C. Myland, K.B. Oldham, J. Electroanal. Chem. 480 (2000) 120.
[9] A.M. Bond, R.J. O'Halloran, I. Ruzic, D.E. Smith, J. Electroanal. Chem. 90 (1978) 381.
[10] C.I. Mooring, H.L. Kies, J. Electroanal. Chem. 78 (1977) 219.
[11] D.E. Smith, Anal. Chem. 48 (1976) 221A, and 48 (1976) 517A.
[12] J.R. Macdonald (Ed.), Impedance Spectroscopy, Wiley, New York, 1987.
[13] S.O. Engblom, P. Sárkány, M. Wasberg, Anal. Instrum. 19 (1990) 181.
[14] J. Hazi, D.M. Elton, A.W. Czerwinski, J. Schiewe, V.A. Vicente-Becket, A.M. Bond, J. Electroanal. Chem. 437 (1997) 1.
[15] J. Schiewe, J. Hazi, V.A. Vicente-Becket, A.M. Bond, J. Electroanal. Chem. 451 (1998) 128.
[16] D. Henderson, J.G. Gordon, J. Electroanal. Chem. 108 (1980) 129.
[17] A.M. Bond, R.J. O'Halloran, I. Ruzic, D.E. Smith, Anal. Chem. 48 (1976) 872.
[18] W.L. Underkofler, I. Shain, Anal. Chem. 37 (1965) 218.
[19] D. Sauer, R. Neeb, Z. Fresenius, Anal. Chem. 290 (1978) 375.
[20] A.C. Michael, R.M. Wightman, C.A. Amatore, J. Electroanal. Chem. 267 (1989) 33.
[21] M. Rudolph, J. Electroanal. Chem. 314 (1991) 13.
[22] M. Rudolph, J. Electroanal. Chem. 338 (1995) 85.
[23] J. Mocak, S.W. Feldberg, J. Electroanal. Chem. 378 (1994) 31.
[24] S.W. Feldberg, C.I. Goldstein, J. Electroanal. Chem. 397 (1995) 1.
[25] D.J. Gavaghan, J. Electroanal. Chem. 420 (1997) 147.
[26] D. Britz, Digital Simulation in Electrochemistry, second ed., Springer, Heidelberg, 1988.
[27] A.M. Bond, U.S. Flego, Anal. Chem. 47 (1975) 2321 and references cited therein.
[28] H.J. Nussbaumer, Fast Fourier Transform and Convolution Algorithms, Springer-Verlag, New York, 1982.
[29] Using MATLAB 5.2, The MathWorks Inc., Natick, MA, 1998.